Phonon Dispersions in Niobium Determined by X-ray Transmission Scattering

M. Holt,[1,2] P. Czoschke,[1,2] H. Hong,[1] P. Zschack,[1] H. K. Birnbaum,[1] T.-C. Chiang[1,2]
[1]Frederick Seitz Materials Research Laboratory and [2]Department of Physics,
University of Illinois at Urbana-Champaign, Urbana, IL, U.S.A.

Introduction

Quasielastic x-ray scattering from thermally populated phonons in crystalline niobium was recorded by using a charge-coupled device (CCD) over a large angular range. The patterns of thermal diffuse scattering (TDS), displayed on a logarithmic intensity scale, reveal rich features. Theoretical patterns based on a lattice dynamics calculation are generated, and a least-squares simultaneous fit of these patterns recorded at several incidence angles yields the phonon dispersion relations over the entire reciprocal space. The dispersions along high-symmetry directions are generally in good accord with available neutron scattering data.

Methods and Materials

Our experiment was performed at the undulator beamline of the University-National Laboratory-Industry Collaborative Access Team (UNI-CAT) at the APS. A transmission Laue geometry was employed, in which an 18.7-keV beam was sent through a crystalline Nb foil with a thickness of 0.1 mm. The foil crystal was prepared by prolonged vacuum annealing of a high-purity polycrystalline foil, resulting in recrystallization over much of the area to form a single crystal oriented with the [110] direction normal to the foil surface. A CCD was used as an area detector, positioned behind the sample to record the transmission scattering images with an exposure time of 5 s each. The incident beam was polarized in the horizontal direction. Data were taken with the sample in air.

Figure 1 shows experimental images of Nb taken (a) at near normal incidence to the crystal, (b) with the crystal rotated 20° around an arbitrary axis, and (c) with the crystal rotated 40° around the same axis. The total data acquisition time for the entire experiment was about 15 s. These images are displayed on a logarithmic intensity scale in order to bring out weak features that are otherwise not visible to the eye. Images (d) through (f) are the corresponding theoretical images (discussed below). The intensity pattern in each case is a result of x-ray scattering from thermally populated phonons. Figure 1(a) exhibits a twofold rotational symmetry and reflection symmetries around the horizontal and vertical axes, while the other two patterns reveal no apparent symmetries because of the arbitrary rotations. By virtue of the wavelength selected, the Bragg condition is never satisfied over the entire area of detection in each case. Thus, none of the bright spots are caused by crystal diffraction.

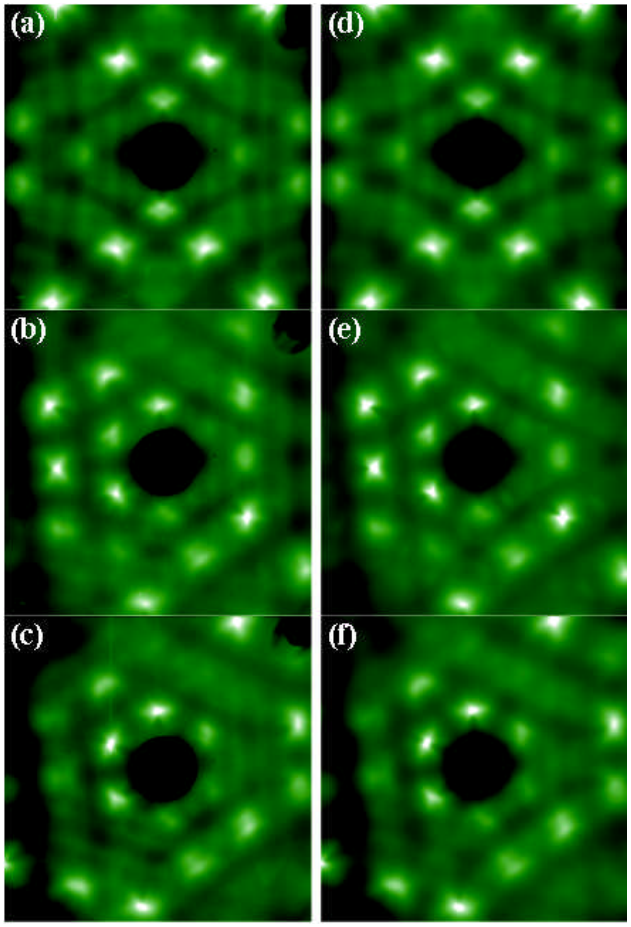

FIG. 1. Transmission x-ray scattering images taken from Nb(110) (a) at near normal incidence, (b) with the sample rotated 20^o around an arbitrary axis, and (c) with the sample rotated 40^o around the same axis. In each case, the shadows of a beam stop in the center of the image and a suspension post in the upper right corner are evident. The corresponding calculated images based on a best simultaneous fit are shown in images (d) through (f).

Results

The theoretical pictures shown in images (d) and (e) of Fig. 1 are derived from a force constant formalism of lattice dynamics, also known as the Born-von Karman model as described in standard textbooks. Force constants up to the eighth nearest neighbors are included in a harmonic lattice model, and diagonalizing this dynamic matrix results in the phonon eigen modes over the entire Brillouin zone. The intensity of scattering by an unpolarized incident x-ray at a certain momentum transfer $\boldsymbol{q}$ is given by a sum over the contributions from the three phonon branches [1]:

$$I_0 \propto f^2 e^{-2M(\mathbf{q})} \sum_{j=1}^{3} \frac{\left|\mathbf{q} \cdot \hat{\mathbf{e}}_j(\mathbf{q})\right|^2}{\mathrm{w}_j(\mathbf{q})} \coth\left(\frac{\hbar \mathrm{w}_j(\mathbf{q})}{2k_B T}\right). \quad (1)$$

In this equation, f = the atomic scattering factor taken from standard x-ray tables, M = the Debye-Waller factor calculated by using the same force constant model, ω = the phonon frequency, $\hat{\mathbf{e}}$ = the polarization vector of the phonon mode, k_B = the Boltzmann constant, T = the sample temperature (300K), and j = the index for the three acoustic phonon branches. The hyperbolic cotangent function in this equation represents a sum of the Bose-Einstein distribution function and the zero-point mode occupancy.

The calculated intensity in each pixel, on a logarithmic scale, is given by:

$$I_{theory} = \log\Big\{\cos^3(2\theta)\cdot T(\theta,\phi) \Big(\Big[\sin^2\phi + \cos^2\phi\cdot\cos^2(2\theta)\Big] (A\cdot I_0 + B) + C(\theta)\Big) + D\Big\} \quad . \quad (2)$$

In this equation, ϕ = the azimuthal angle between the plane of polarization of the incident beam and the scattering plane and 2θ = the scattering angle. The expression within the brackets containing these angles accounts for the linear polarization of the incident beam. The quantity A = an intensity normalization factor; B = a constant background from higher order and defect scattering from the sample; C = a slowly varying sample-generated background, including the tabulated Compton scattering for Nb (interpolated at each pixel) plus sample fluorescence represented by a Lorentzian; and D = an overall constant background related to the detector noise and response. The sample attenuation $T(\theta,\phi)$ is calculated by using the distances traveled by the incident and scattered beams for the particular sample orientation. One factor of cos(2θ) on the left side of the formula is for solid angle conversion associated with planar projection, and the additional $\cos^2(2\theta)$ factor allows for the inverse square distance dependence of the scattering intensity from the sample to different points on the detector plane.

Equations (1) and (2) are used to generate theoretical images, and these are used in a least-squares, pixel-by-pixel fit to all three experimental images simultaneously. The areas in the images around the beam stop and the support post in the upper right corner were removed from the fit via a mask function. The fitting parameters include *A*, *B*, *C*, and *D* above; the three Euler angles determining the sample orientation; the exact distance from the sample to the CCD screen; the x and y position of the screen relative to the beam; and the Born-von Karman force constants. The fitting of calculated images to the data can essentially be thought of as numerically solving Eq. (1) to reproduce the phonon frequencies as a function of momentum transfer.

The phonon dispersions along high-symmetry directions obtained from the best fit are shown in Fig. 2(a) by the solid curves. These compare fairly well with the circles, which represent results deduced from neutron scattering. The agreement is very good at low frequencies, but at high frequencies, there are noticeable differences in certain regions in the Brillouin zone, with the maximum deviation up to about 10%. The overall fit is certainly not quite as good as in the case of Si that was previously reported [2], which might be due to a confluence of several factors that affect the analysis. First, because of the anomalies in the dispersion, very long range forces are needed to obtain a reasonable description of the phonon dispersion curves [3-7]. It is known that even the eighth nearest neighbor Born-von Karman model cannot reproduce all the features seen in the neutron data when fit directly. Thus, some discrepancies are expected. Second, it has been suspected that the shortfall of the force constant model might get worse as one moves away from the high-symmetry directions probed in the neutron studies. Since the bulk of our TDS data are taken from regions in the reciprocal space off the high-symmetry directions, the limitations of the model can be exacerbated when the comparison is made only along high-symmetry directions.

Discussion

In summary, the present work offers a test of the TDS method, and fairly satisfactory results were obtained for a system whose lattice dynamics have been the subject of intensive studies. The “swoop” anomaly that is the focus of numerous previous studies is accurately reproduced. The crystalline quality of our Nb foil sample cannot be compared with that of the Si wafers used in previous studies, but the slightly worse fit here is unlikely to be sample-related. Rather, the limitations of the force constant model and the imperfections of the CCD as a detector appear to be the main issues. None of these are fundamental in nature, and they can be overcome as the

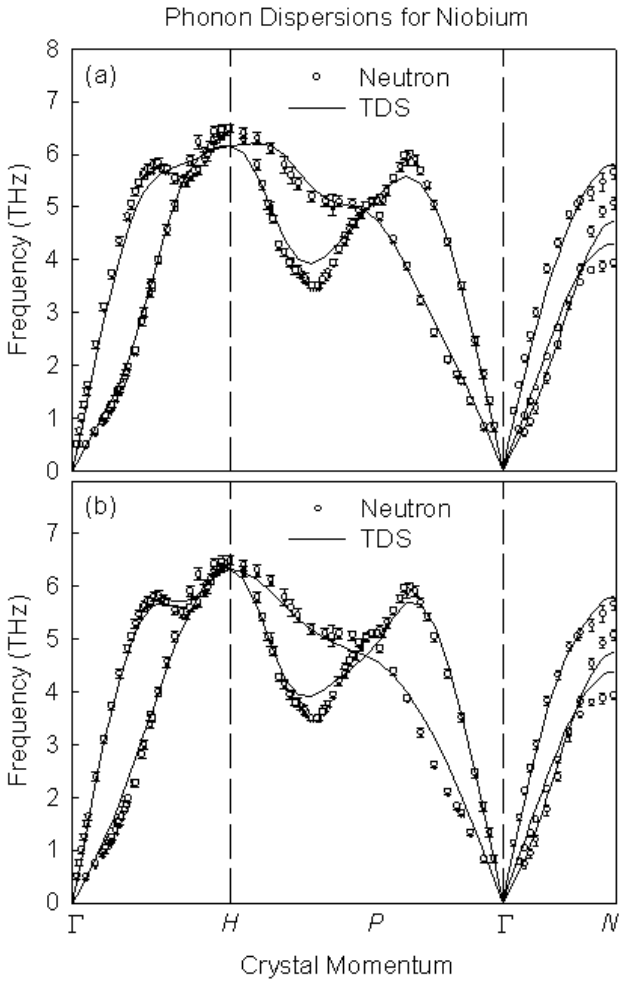

FIG. 2. Phonon dispersion curves of Nb. Open circles with error bars are neutron scattering data from Reference 7. Solid curves are derived from a best fit to the TDS patterns based on a lattice dynamic calculation using (a) an eighth nearest neighbor Born-von Karman model and (b) a third nearest neighbor Born-von Karman model modified to account for charge fluctuation.

methods get further refined. A significant advantage of the TDS method is its efficiency (the entire data acquisition time for this experiment is just 15 s, and the data cover a very wide range in the reciprocal space). No special efforts were required to align and orient the sample. This work thus illustrates both the powers and the limitations of the TDS method for materials studies.

Acknowledgments

We gratefully acknowledge the use of the UNI-CAT facility at the APS. Use of the APS was supported by the U.S. Department of Energy, Office of Science, Office of Basic Energy Sciences, under Contract No. W-31-109-ENG-38.

References

[1] B. E. Warren, *X-ray Diffraction* (Dover, New York, NY, 1969).

[2] M. Holt, Phys. Rev. Lett. **83**, 3317 (1999); M. Y. Chou and M. Choi, ibid. **84**, 3733 (2000); M. Holt and T.-C. Chiang, ibid. **84**, 3734 (2000).

[3] P. H. Dederichs and H. Schober, *Landolt Bornstein* NS Group III **13a** (Springer-Verlag, Berlin, Germany, 1981), p. 96. This article contains a detailed list of references and a review of lattice dynamics models and neutron scattering results.

[4] Y. Nakagawa and A. D. B. Woods, Phys. Rev. Lett. **11**, 271 (1963).

[5] R. I. Sharp, J. Phys. C **2**, 421 (1969).

[6] B. M. Powell, A. D. Woods, and P. Martel, *Neutron Inelastic Scattering*, Vol. 43 (International Atomic Energy Agency, Vienna, Austria, 1972).

[7] F. Guthoff, B. Hennion, C. Herzig, W. Petry, H. R. Schober, and J. Trampenau, J. Phys.: Condens. Matter **6**, 6211 (1994).